processes

MDPI

Article

Experimental and Kinetic Simulations of Technetium-Catalyzed Hydrazine Oxidation in Nitric Acid Solution

Ting Yu, Hu Zhang *, Yongzhi Ning, Hongling Li, Ziteng Gao, Bo Wang and Zhijun Cen

China Institute of Atomic Energy, Beijing 102413, China; 13667132765@163.com (T.Y.); tataning@163.com (Y.N.); 13551584569@163.com (H.L.); gzt15822528462@163.com (Z.G.); wangbosmile@126.com (B.W.); cenzj2018@163.com (Z.C.)

* Correspondence: ciaezhhu@163.com

Abstract: The catalytic reaction of Tc plays a significant role in the chemical separation process during spent fuel reprocessing. However, few studies have been conducted on the chemical reaction mechanism between Tc and hydrazine. Moreover, the instability of Tc(V) and Tc(VI) makes their measurement difficult, rendering many aspects of the reaction process and mechanism unclear. This study investigates the catalytic reaction between Tc and hydrazine in a nitric acid solution. To this end, we obtained the kinetic laws of the reaction under various conditions of acidity, hydrazine concentration, and Tc concentration by monitoring the concentrations of hydrazine and Tc(VII) over time. The reaction kinetics model demonstrated that numerical simulations could effectively predict the reaction process. Results indicated that hydrazine promotes the reduction of Tc(VII) to Tc(IV), constituting the basis for establishing the Tc(IV, V, VI, VII) catalytic cycle. Among these, Tc(V) and Tc(VI) were important active intermediates and the main consumers of hydrazine. The research results may be useful for actinide separation processes based on valence control.

Keywords: Tc; hydrazine; catalytic reaction; numerical simulation; nuclear fuel reprocessing

check for updates

Citation: Yu, T.; Zhang, H.; Ning, Y.; Li, H.; Gao, Z.; Wang, B.; Cen, Z. Experimental and Kinetic Simulations of Technetium-Catalyzed Hydrazine Oxidation in Nitric Acid Solution. *Processes* **2024**, *12*, 2319. https://doi.org/10.3390/pr12112319

Academic Editor: Maria Victoria López Ramón

Received: 12 September 2024
Revised: 6 October 2024
Accepted: 10 October 2024
Published: 23 October 2024

Copyright: © 2024 by the authors. Licensee MDPI, Basel, Switzerland. This article is an open access article distributed under the terms and conditions of the Creative Commons Attribution (CC BY) license (https://creativecommons.org/licenses/by/4.0/).

1. Introduction

Nuclear fission energy is generated by the process of a heavy atomic nucleus undergoing a fission reaction in response to neutron bombardment, resulting in the release of a substantial amount of energy. It offers several advantages, including low carbon output, high energy density, and the potential for recycling renewable fuels. Consequently, in the pursuit of carbon neutrality, nuclear fission energy is increasingly recognized as an efficient and clean low-carbon energy source. The large-scale development of nuclear fission energy generates a considerable amount of spent fuel while providing clean energy [1]. ^{99}Tc in spent fuel is a long-lived radionuclide with a half-life of 2.13×10^5 years. In the spent fuel of a light-water reactor with a burn-up of 45 GWd/t HM, the content of ^{99}Tc is approximately 1 kg/t HM [2]. As nuclear fuel burn-up progresses, the content of ^{99}Tc in the spent fuel markedly increases. Tc is highly mobile and easily migrates under geological disposal conditions [3,4], posing long-term potential hazards to ecosystems, thereby garnering significant attention in spent fuel reprocessing.

Currently, the Pu U reduction extraction (PUREX) process is the primary method for reprocessing, whereby tributyl phosphate (TBP) is used as an extractant to separate U and Pu from nitric acid solutions of spent fuel. The PUREX process primarily comprises three stages: the U–Pu co-decontamination, Pu purification, and U purification cycles. The solution initially enters the co-decontamination cycle, in which U and Pu are extracted by TBP, and Tc, in the form of TcO_4^-, is co-extracted along with Zr^{4+}, UO_2^{2+}, and Pu^{4+}. In the subsequent U–Pu separation stage, U(IV) and hydrazine are commonly used as reductants, where hydrazine scavenges nitrous acid, and the reductant is utilized to reduce Pu(IV) in the TBP organic phase to Pu(III) to complete the U–Pu separation. However, in the presence

of Tc, 5–8 times more U(IV) than the stoichiometry of the chemical reaction must be added to ensure the effective reduction of Pu(IV), mainly because of the catalytic effect of Tc [5–8]. Therefore, a step for washing Tc must be added before the U–Pu separation unit to limit the catalytic effect of Tc, further complicating the process flow. To suppress the catalytic effect of Tc, a Russian RT-1 reprocessing plant tested the addition of diethylenetriamine pentaacetic acid (DTPA) and hydrazine to a U–Pu separation tank. The use of DTPA to chelate Tc(IV) effectively suppresses the catalytic behavior of Tc, and the separation coefficient of SF (Tc/U) in the U–Pu separation unit reaches 350–500 [9,10]. In recent years, many countries have focused on enhancing the PUREX process to utilize U resources efficiently and minimize nuclear waste. A key objective is the quantitative separation of Tc and Np, achieving an extraction rate exceeding 99%. For example, the UREX process, developed in the United States, employs acetohydroxamic acid (AHA) as a complexing/reducing agent. AHA acts on a dissolved solution of spent fuel during the extraction phase, where Pu and Np along with minor actinides, americium, and curium, enter the extraction residue. While U and Tc are extracted using TBP and then enter the organic phase, Tc is first washed off with nitric acid, and then U is extracted with washed nitric acid. Finally, the UREX process obtains three products, respectively, Pu products containing Np, Tc products (>99% Tc), and U products (>99.9% U) [11,12]. Existing studies have shown that the valence state of Np changes with that of Tc during catalytic reactions. Hence, the quantitative control of Np in the PUREX process becomes more challenging [13–15].

Although the catalytic reaction of Tc is crucial for reprocessing, few studies have investigated the chemical reaction mechanism between Tc and hydrazine. Garraway et al. [8] suggested that Tc functions as a catalyst and that the reaction process can be divided into three stages: the induction, fast reaction, and termination periods. During the induction phase, hydrazine slowly reduces Tc(VII) to Tc(VI), and the generated Tc(VI) is reduced to Tc(IV) through double-electron reduction. Tc(IV) and Tc(VII) react to form unstable Tc(V) and Tc(VI), respectively, which then rapidly react with hydrazine to form Tc(IV) and enter the rapid reaction phase. With a significant consumption of hydrazine, the reaction enters the termination phase. However, the measurement of unstable Tc(V) and Tc(VI) values is challenging, and many aspects regarding the reaction process and mechanism remain unclear. Based on experimental research, this study refined the reaction system and conducted simulations to model the complex catalytic reactions. Kinetic parameters were analyzed, and key rate-limiting steps were determined to enhance the understanding of the reaction mechanism. The study provides insights for optimizing processes in nuclear reprocessing plants, potentially improving the efficiency and safety in the separation of valuable nuclides from nuclear spent fuel. It offers strategies to control and mitigate the environmental impact of Tc, a long-lived radionuclide, by understanding its behavior and the potential catalytic processes that affect its mobility and environmental persistence.

2. Experiments and Methods

^{99}Tc is a long-lived radioactive nuclide with a half-life of 2.13×10^5 years, posing a long-term radiotoxicity threat to the ecological environment. Therefore, Tc experiments must be conducted in a sealed glove box to prevent Tc from leaking into the environment. The Tc(VII/VI/V/IV) mentioned in this article represents only the valence state of Tc and does not represent its chemical form.

The reagents used in the experiments were 65%–68 wt% nitric acid (National Pharmaceutical Group, analytically pure), 17 g/L ammonium pertechnetate (Tc) (Oak Ridge National Laboratory, Oak Ridge, TN, USA), and hydrazine hydrate (Sinopharm Group, analytically pure). The Ocean Optics HR4Pro high-resolution fiber-optic spectrometer (Ocean Optics, Orlando, FL, USA)- and Horiba iHR550 modular Raman spectrometer (Horiba, Japan) were used for the measurements.

2.1. Experiments

The experiment is divided into three parts: one is the kinetic study of the reaction between technetium and hydrazine: changing the concentration of hydrazine, technetium, and nitric acid to obtain reaction kinetics data; the second is to change the reaction temperature to obtain the activation energy for the reaction between technetium and hydrazine; and the third is to obtain the technetium in the intermediate valence state by constant potential electrolysis.

2.2. Analytical Methods

To determine the activity of ^{99}Tc in the samples, the aliquots of investigated TcO_4^- solutions were assayed by a liquid scintillation counting method (instrument used: Perkin Elmer Tri-Carb 2910TR, PerkinElmer, Shelton, CT, USA) using Ultima Gold liquid scintillator cocktail. The reported activity is the average of the values measured for three samples collected from each of the investigated solutions. The concentration of hydrazine was analyzed by a spectrophotometric method using p-dimethylaminobenzaldehyde as the chromogenic agent. The changes in the absorbance value at 457 nm were measured using an Ocean Optics HR4Pro High-Resolution Fiber Optic Spectrometer (Ocean Optics, Orlando, FL, USA), and the concentration of hydrazine was calculated based on the standard working curve.

3. Numerical Modeling

The rate equations for each reaction were included in a set of molar balances for a batch reactor resulting in a set of ordinary differential equations. Use the fourth-order Runge Kutta method (ode45) for numerical solution. The initial values of the calculations were set such that only the concentrations of nitric acid, hydrazine, and Tc(VII) under the initial reaction conditions were considered. The concentrations of the remaining components were set to zero.

4. Results and Discussion

4.1. Experimental Results

In the PUREX process, to ensure a sufficiently fast Pu reduction reaction rate, the concentration of nitric acid in the stripping solution was maintained within the range of 0.5–1.5 mol/L [16,17]. At a burn-up of 33 GW day ton^{-1} U the concentration of Tc in the feed solution was 183 mg/L [18]. In the uranium-plutonium separation section, the typical hydrazine concentration was 0.05 mol/L to 0.15 mol/L [13]. Therefore, in the experiment, the nitric acid concentration selected was 1.0 mol/L, and the initial concentrations of TcO_4^- and hydrazine were 1.2 mmol/L and 0.1 mol/L, respectively. The reaction between Tc and hydrazine proceeds as Figure 1 shows.

A strong correlation exists between the changes in the Tc(VII) and hydrazine concentrations (Figure 1). During the induction period (0–70 min), the concentration of hydrazine remained unchanged, and that of the Tc(VII) slowly decreased. However, when the reduced Tc accounts for approximately 10% of the total Tc, the reaction enters the rapid reaction phase. In the rapid reaction stage, with the rapid consumption of hydrazine, the reaction solution gradually turned from colorless to yellow and numerous bubbles appeared. The concentration of the Tc(VII) decreased rapidly, and approximately 60% of the Tc(VII) was reduced after approximately 150 min. Subsequently, the rate of hydrazine consumption gradually decreased until the hydrazine was completely oxidized. Correspondingly, the concentration of Tc(VII) first increased rapidly and then maintained a slowly increasing trend. Specific explanations for this phenomenon will be given in subsequent analyses.

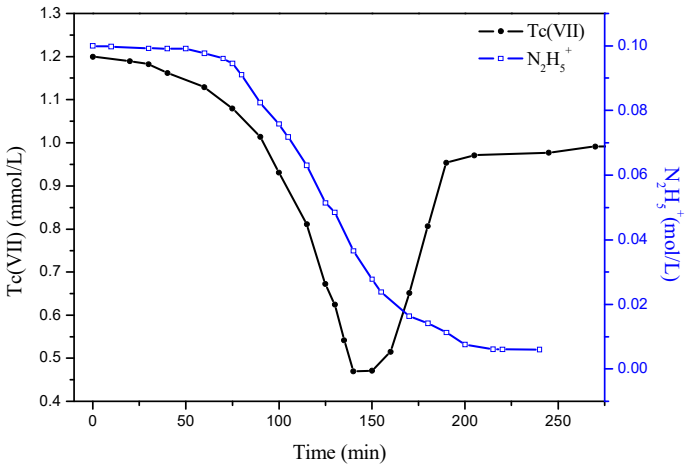


Figure 1. Reaction process of hydrazine and Tc(VII) in nitric acid solution. $c(N_2H_5^+)$ = 0.1 mol/L, $c(TcO_4^-)$ = 1.2 mmol/L, $c(HNO_3)$ = 1.0 mol/L, T = 35 °C.

Figures 2–4 show the dependence of the reaction rate on the hydrazine, TcO_4^-, and nitric acid concentrations. Although an increase in the hydrazine concentration (0.05–0.20 mol/L) does not have a significant effect on the induction period, it increases the rate of the fast reaction period (Figure 2a). Moreover, although no significant change in the reaction rate of Tc(VII) is observed (Figure 2b), the time required for the turning point of the Tc(VII) concentration change is prolonged with an increase in hydrazine concentration, implying that additional time is required to consume hydrazine.

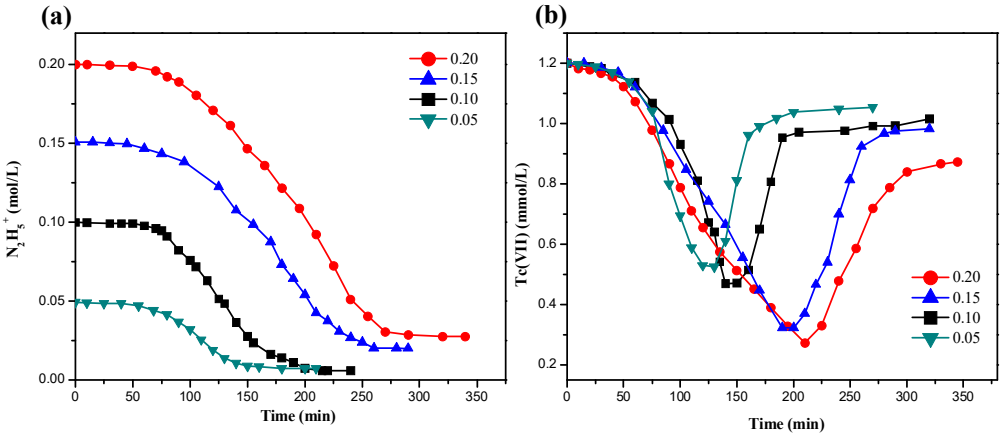


Figure 2. Dependence of hydrazine concentration (**a**), pertechnetate concentration (**b**) on time at various initial concentrations of hydrazine. $c(TcO_4^-)$ = 1.2 mmol/L, $c(HNO_3)$ = 1.0 mol/L, T = 35 °C; $c(N_2H_5^+)$ = 0.2 mol/L, 0.15 mol/L, 0.1 mol/L, 0.05 mol/L.

As the concentration of TcO_4^- increases (0.8–3.0 mmol/L), the induction period of the reaction shortens (Figure 3), the reaction rate of hydrazine significantly accelerates, and the rate of Tc(VII) reduction increases. The time for the turning point of Tc(VII) concentration change also shortens, and the reaction rate of the consumed Tc(VII) being oxidized accelerates. When the concentration of nitric acid increases from 1.0 to 2.0 mol/L (Figure 4a), the induction period of the hydrazine reaction significantly shortens, the reaction rate in the rapid reaction stage is significantly increased, and the residual amount of hydrazine increases. Correspondingly, as Figure 4b shows, the reaction rate of Tc(VII) also increases with increasing acidity, and the amount of reduced Tc decreases with increasing acidity.

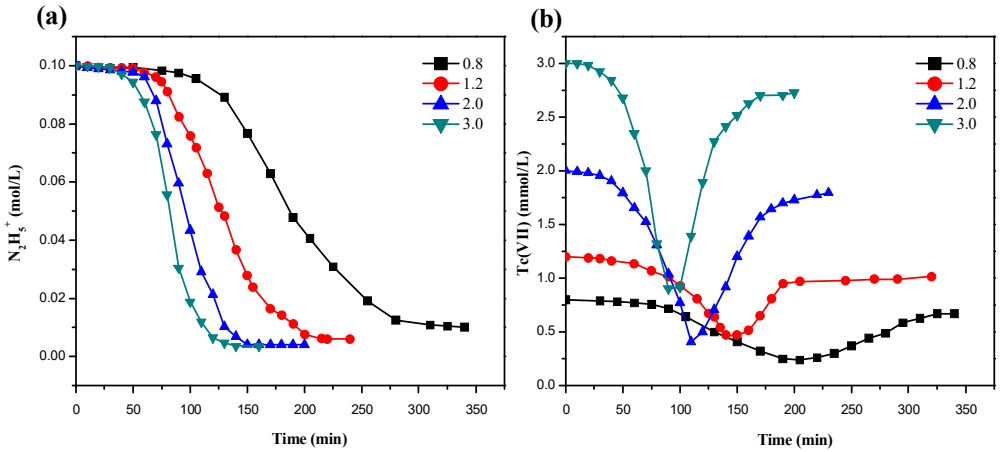


Figure 3. Dependence of hydrazine concentration (**a**), pertechnetate concentration (**b**) on time at various initial concentrations of pertechnetate. $c(N_2H_5^+)$ = 0.1 mol/L, $c(HNO_3)$ = 1.0 mol/L, T = 35 °C; $c(TcO_4^-)$ = 0.8 mmol/L, 1.20 mmol/L, 2.0 mmol/L, 3.0 mmol/L.

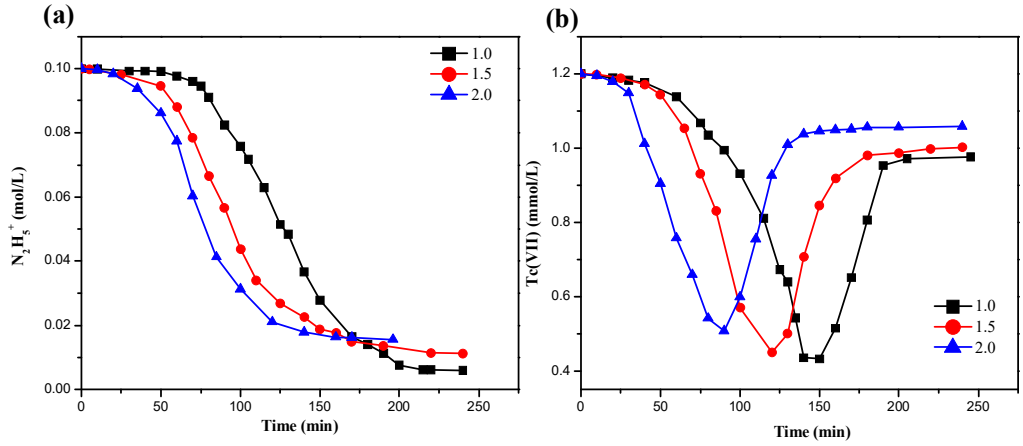


Figure 4. Dependence of hydrazine concentration (**a**), pertechnetate concentration (**b**) on time at various initial concentrations of nitric acid concentrations. $c(TcO_4^-)$ = 1.2 mmol/L, $c(N_2H_5^+)$ = 0.1 mol/L, T = 35 °C; $c(HNO_3)$ = 1.0 mol/L, 1.5 mol/L, 2.0 mol/L.

From the experimental data that Figures 2–4 show, the apparent rate equation for the reaction kinetics of the rapid consumption of hydrazine can be proposed. We assume that the reaction rate can be expressed as

$$r = -\frac{d[N_2H_4]}{dt} = k\left[TcO_4^-\right]^a\left[N_2H_4\right]^b[HNO_3]^c \quad (1)$$

In Equation (1), r is the reaction rate; k is the reaction rate constant, which is temperature dependent; and a, b, and c are the reaction orders of the reactants pertechnetate, hydrazine, and nitric acid, respectively. The differential method was used to plot lg r (lg $[-d[N_2H_4]/dt]$) against lg c(A), where component A denotes N_2H_4, TcO_4^-, and HNO_3, and the slope of the fitted line is the order of component A. The fitted data and obtained reaction orders for each component are listed in the Supplementary Materials. Through the above data processing, the rate equation for this fast reaction stage at 35 °C can be expressed as

$$r = -\frac{d[N_2H_4]}{dt} = 0.72\left[TcO_4^-\right]^{0.37}\left[N_2H_4\right]^{0.81}\left[HNO_3\right]^{0.48}$$

Based on the experiment that Figure 5 shows, when the reaction temperature is increased from 30 to 45 °C, the induction period of the reaction between hydrazine and Tc is shortened or even eliminated, and the rate of the rapid reaction phase is accelerated. The data for hydrazine in the fast reaction phase were processed using the Arrhenius equation and plotted against ln (k) and 1/T. The activation energy in the fast reaction phase can be obtained from the slope as 60.10 ± 1.42 kJ/mol.

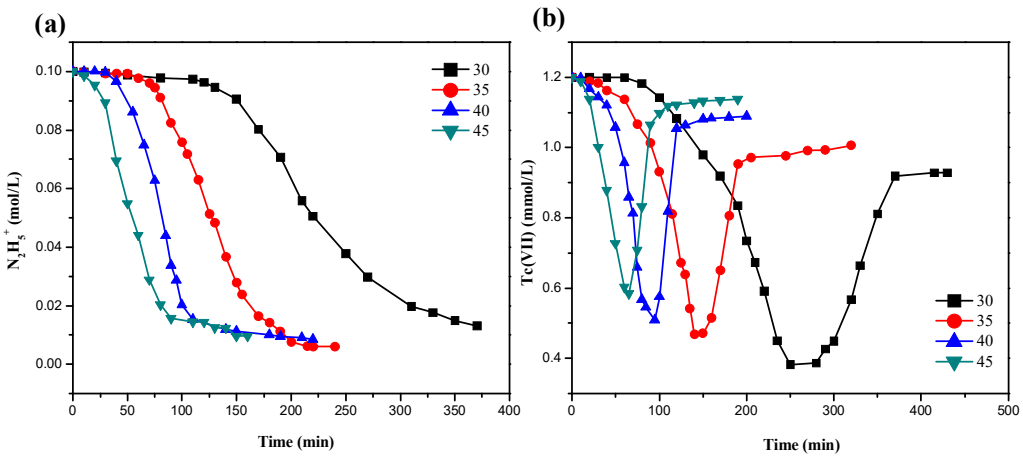


Figure 5. Dependence of hydrazine concentration (**a**), pertechnetate concentration (**b**) on time at different temperatures. $c(TcO_4^-)$ = 1.2 mmol/L, $c(N_2H_5^+)$ = 0.1 mol/L, $c(HNO_3)$ = 1.0 mol/L; T = 30 °C, 35 °C, 40 °C, 45 °C.

In the reaction kinetic Equation (1), because the reaction orders of hydrazine, nitric acid, and TcO_4^- are not integers, complex chemical reactions occur between hydrazine and Tc in the nitric acid solution. Consequently, the reaction process exhibits non-linear kinetic behavior. The reaction order of TcO_4^- is 0.37, which is significantly lower than that of hydrazine at 0.81, indicating that most TcO_4^- does not directly participate in the oxidation of hydrazine but catalyzes the reaction with hydrazine by forming an active intermediate valence state Tc(V, VI).

The intermediate valence state of Tc(Tc(V) or Tc(IV)) was obtained by the constant potential electrolytic reduction of Tc(VII) at a potential of −0.10 V (vs. saturated calomel electrode (SCE)) and characterized by UV-vis and Raman spectroscopy. The detailed experimental procedure is described in the Supplementary Material. Figure 6 presents the UV-vis spectra of the electrolyte measured at electrolysis times of 0, 30, 90, and 110 min. The absorption at 263 nm (the characteristic absorption of Tc(VII) in nitric acid solution), which is affected by the characteristic absorption of HNO_3, did not change significantly with the electrolysis time. The absorption at 311 nm, which is the characteristic absorption of Tc(IV) [19–21], gradually increased with increasing electrolysis time, indicating that during the electrolysis process, Tc(VII) was continuously reduced to Tc(IV).

Figure 7 shows the Raman spectra measured after four dilutions of the electrolyte at 0, 30, and 90 min of the electrolytic reduction. The N–O stretching vibration of this species is located at 1046 cm^{-1}, and the H–O bend is located at 1630 cm^{-1}. TcO_4^- has a tetrahedral structure and belongs to the Td point group, with the characteristic signal at 910 cm^{-1}. Grey [22] reported that vibration frequencies for $[O{=}M{=}O]^{n+}$ and $[M{\equiv}O]$ stretching modes typically range from 870 to 920 cm^{-1} and from 950 to 1000 cm^{-1}, respectively, where M represents Re. The appearance of Raman shifts between 972, 1172, and 1181 cm^{-1} after 90 min of electrolysis indicates the formation of Tc in the intermediate valence state (Figure 7). Combining these with the results obtained from the UV-Vis spectroscopy, we speculated that the peaks at 1172 and 1181 cm^{-1} may correspond to Raman shifts indicative of different forms of Tc(IV) [23]. The shift 972 cm^{-1} is located in the range 950–1000 cm^{-1}, which may be attributed to the vibration of Tc(V). Tc(V) may exist in the form of TcO^{3+} and TcO^{2+} in the solution, where the Tc–O bond in TcO^{3+} contains two π bonds and one

σ bond, indicating that Tc(V) exists in the form of TcO^{3+}in the solution. At an extremely low potential (−0.10 V), Tc(VII) undergoes a reaction on the electrode to obtain three electrons and is directly reduced to Tc(IV). Therefore, the Tc(V) that appears in the solution should originate from the reaction between Tc(IV) generated on the electrode and Tc(VII) in the solution.

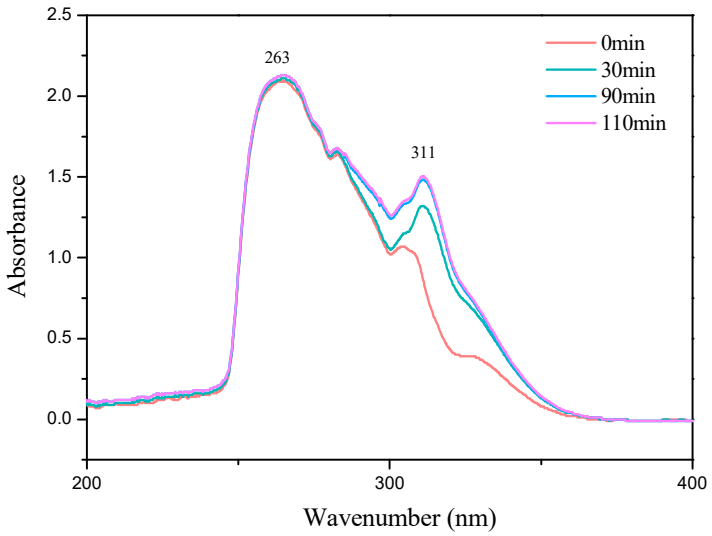


Figure 6. Time dependence of the UV-visible absorption spectra of the electrolysis reaction. $c(HNO_3)$ = 0.2 mol/L, c(Tc(VII)) = 80.0 mmol/L, T = 35 °C.

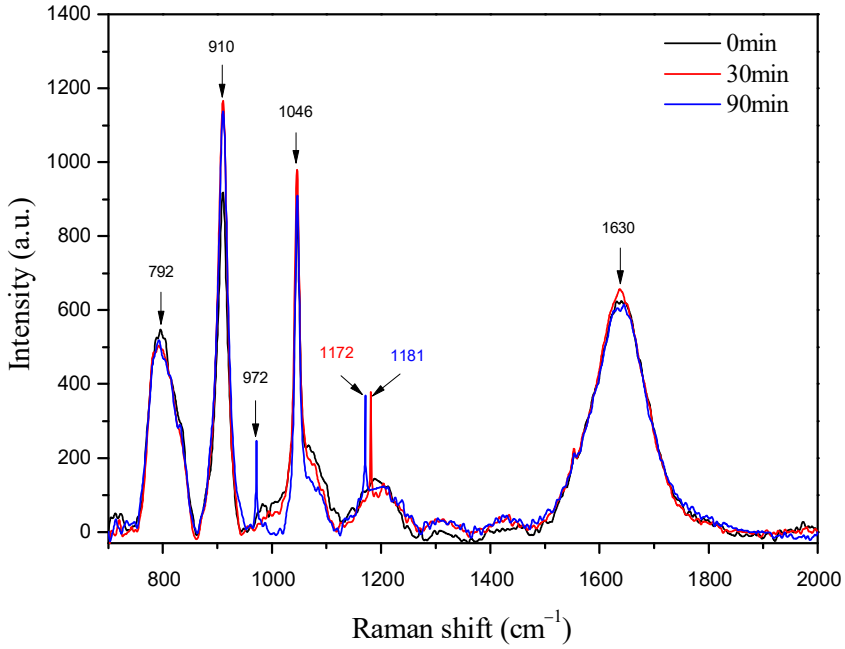


Figure 7. Raman spectrum of technetium reduced by electrolysis. $c(HNO_3)$ = 0.2 mol/L, c(Tc(VII)) = 80.0 mmol/L, T = 35 °C.

4.2. Numerical Simulation Results

Chemical reactions are essentially the result of the collective interactions within a system; the main focus of this study was determining the reaction mechanism that leads to the observed behavior of hydrazine and Tc. However, most reactants cannot easily be identified and measured because of the complex catalytic reactions involved. Moreover, the complex reaction mechanism cannot easily be explored by simply analyzing the changes in

hydrazine and Tc(VII) concentrations in experiments. Therefore, numerical simulations of reaction kinetics are required to understand the reaction process and mechanism.

Based on the above analysis, Table 1 presents the kinetic models of these reactions. Among these, reactions 1–3 are the gradual reduction of Tc(VII) to Tc(IV) by hydrazine. Correspondingly, reactions 4–6 are the gradual oxidation of Tc(IV) to Tc(VII) by nitric acid. Reactions 7 and 8 represent the valence transition of Tc, which is key to the catalytic reaction. Reaction 9 is the reaction between hydrazine and nitrous acid, as the hydrazine concentration is due to an excess of nitrous acid, and the reaction products are N_2O and N_2. The oxidation product of hydrazine is expressed uniformly as $N_2H_{4(OX)}$.

Table 1. Equations used in the simulation of the Tc-$N_2H_5NO_3$-HNO_3 reaction.

No.	Reaction	Rate Equations	k_i/(mol^{-1}·min^{-1}) 35 °C	Ref.
1	Tc(VII) + N_2H_4 → Tc(VI) + $N_2H_{4(OX)}$	$\nu_1 = k_1[Tc(VII)][N_2H_4]$	3.3×10^{-4}	[8]
2	Tc(VI)+ N_2H_4 → Tc(V) + $N_2H_{4(OX)}$	$\nu_2 = k_2[Tc(VI)][N_2H_4]$	12.5	
3	Tc(V)+ N_2H_4 → Tc(IV) + $N_2H_{4(OX)}$	$\nu_3 = k_3[Tc(V)][N_2H_4]$	12.5	[8]
4	Tc(IV)+ HNO_3 → Tc(V)+ HNO_2	$\nu_4 = k_4[Tc(IV)]\ [HNO_3]$	1.19	
5	Tc(V)+ HNO_3 → Tc(VI)+ HNO_2	$\nu_5 = k_4[Tc(IV)]\ [HNO_3]$	0.167	
6	Tc(VI)+ HNO_3 → Tc(VII)+ HNO_2	$\nu_6 = k_6[Tc(IV)]\ [HNO_3]$	0.033	[8]
7	Tc(IV) + Tc(VII) → Tc(V) + Tc(VI)	$\nu_7 = k_7[Tc(IV)][Tc(VII)]$	350	
8	Tc(V) + Tc(VI) → Tc(IV) + Tc(VII)	$\nu_8 = k_8[Tc(V)][Tc(VI)]$	340	
9	$2HNO_2$+ N_2H_4 → N_2O +N_2 +$3H_2O$	$\nu_9 = k_9\ [HNO_2]\ [N_2H_4]$	4871	

The rate equations used to calculate the concentrations of Tc(VII, VI, V, and IV), N_2H_4, HNO_2, and HNO_3 are as follows:

$$d[Tc(VII)]/dt = \nu_6 - \nu_1 - \nu_7 + \nu_8$$

$$d[Tc(VI)]/dt = \nu_1 - \nu_2 + \nu_5 - \nu_6 + \nu_7 - \nu_8$$

$$d[Tc(V)]/dt = \nu_2 + \nu_4 - \nu_3 - \nu_5 + \nu_7 - \nu_8$$

$$d[Tc(IV)]/dt = \nu_3 - \nu_4 - \nu_7 + \nu_8$$

$$d[N_2H_4]/dt = -\nu_9 - \nu_1 - \nu_2 - \nu_3$$

$$d[HNO_2]/dt = \nu_4 + \nu_5 + \nu_6 - 2\nu_9$$

where ν_i (i = 1, 2, . . ., 9) represents the reaction rate of each reaction equation presented in Table 1.

The optimum rate constants (Table 1) were obtained using the following method: The standard deviation (SD) between the experimental and simulated hydrazine concentrations over time was summed and termed the summed standard deviation (represented as SSD in this article). The smaller the SSD value, the more consistent the simulated value is with the experimental value. The SSD of each rate constant was calculated to be within ±40% of its range. Once the minimum of SSD value is calculated, the optimum rate constant for each reaction can be obtained.

The change in k_1–k_3 does not cause a change in the SSD values (Figure 8) indicating that reactions 1, 2, and 3 have a minimal effect on the overall reaction rate. Therefore, during the induction phase, Tc(VII) is reduced to Tc(IV) through a gradual electron transfer. For k_4–k_8, the change in k_7 causes the greatest change in SSD and has the greatest impact on the overall reaction rate. Therefore, reaction 7 is the rate-determining step of the reaction process, indicating that the consumption of hydrazine originates from the catalytic effect of Tc. k_4, k_5, and k_6 correspond to the reactions of Tc(IV), Tc(V), and Tc(VI) with nitric acid, respectively. The reaction rate k_9 between the produced nitrous acid and hydrazine is extremely fast. Therefore, the consumption of hydrazine by these three reactions cannot be ignored.

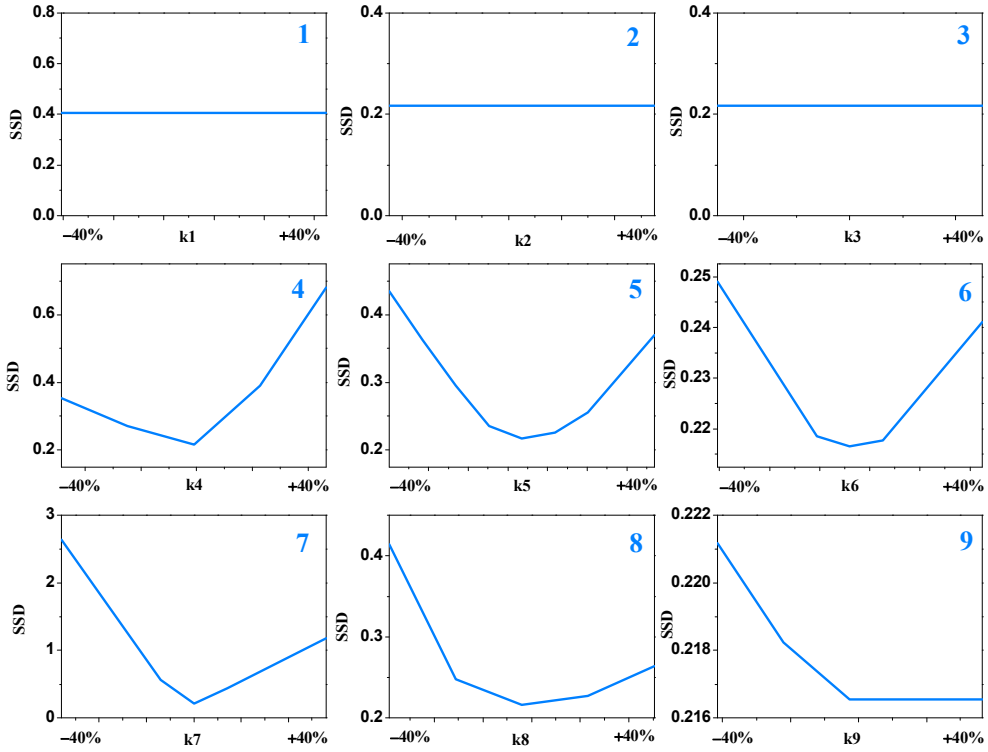


Figure 8. Sensitivity analysis results for each reaction's kinetic parameter. Numbers 1–9 correspond to reactions 1–9 in Table 1.

Calculations showed that the introduction of reaction 8 reduced the SSD from 0.602 to 0.216 and that reaction 8 was consistent with the experimental results. Kuznetsov [24] reported that in non-complexing media, Tc(V) and Tc(VI) are thermodynamically unstable and disproportionate to Tc(IV) and Tc(VII).

$$3TcO_4^{2-} + (2 + x)\ H_2O \rightarrow 2TcO_4^{-} + TcO_2{\cdot}xH_2O + 4OH^{-}$$

$$3TcO_3^{+} + (5 + x)\ H_2O \rightarrow TcO_4^{-} + 2TcO_2{\cdot}xH_2O + 10H^{+}$$

Combining both equations yields reaction 8-. This indicates that during the catalytic reaction, Tc(IV) and Tc(VII) can react rapidly to form Tc(V) and Tc(VI), and Tc(V) and Tc(VI) can also react relatively rapidly to form Tc(IV) and Tc(VII), respectively. Although Tc(V) and Tc(VI) have low concentrations and short lifetimes, they exhibit high activities and are active intermediates for establishing nonassociative catalytic activation cycle reactions.

Figure 9 shows a comparison between the simulated and experimental values of the reaction at nitric acid concentrations of 1.0, 1.5, and 2.0 mol/L. The sum of the standard deviations (SSD) of the simulated and experimental values of hydrazine concentration over time was calculated to be 0.217, 0.510, and 0.557 when the nitric acid concentration was 1.0 mol/L, 1.5 mol/L, and 2.0 mol/L, respectively, and the SSD values were small indicating that the calculated results of the hydrazine consumption curve were consistent with the experimental values. The trend of the concentration change in Tc(VII) was consistent with the experimental results, proving the validity of the simulation.

Figure 10 shows the dependence of the Tc-normalized concentration over time obtained from the simulation calculations. As observed in plots A and B (Figure 10), the hydrazine and nitrous acid concentrations show a close correspondence over time. The entry of the reaction from the induction period (0–70 min) into the fast reaction period was marked by a rapid increase in nitrous acid concentration from zero. Accordingly, the rate of hydrazine consumption begins to accelerate as indicated by reaction 9 (Table 1). As nitrous acid is produced by reactions 4, 5, and 6 (Table 1), that is, the reaction of Tc(IV, V, VI) with nitric

acid, an increase in both the initial Tc(VII) and nitric acid concentration accelerates the generation of nitrous acid, thus shortening the induction period.

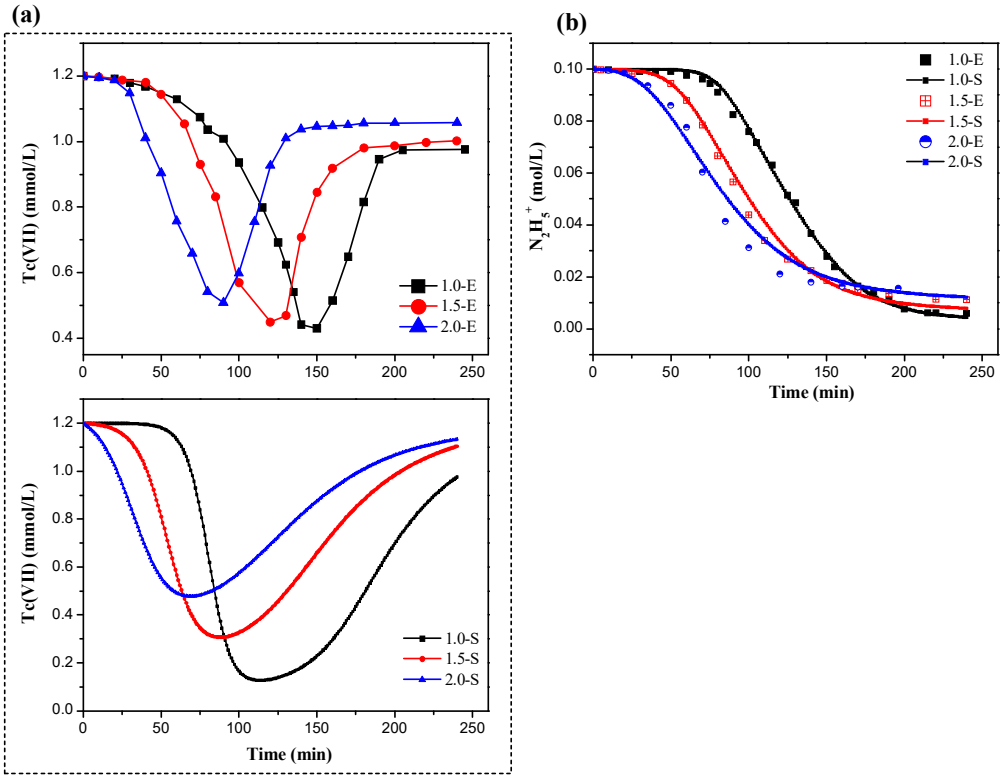


Figure 9. Simulated and experimental values of the dependence of pertechnetate concentration (**a**), hydrazine concentration (**b**) on time at various initial concentrations of nitric acid. $c(TcO_4^-)$ = 1.2 mmol/L, $c(N_2H_5^+)$ = 0.1 mol/L, T = 35 °C; $c(HNO_3)$ = 1.0 mol/L, 1.5 mol/L, 2.0 mol/L, 3.0 mol/L.

When the nitrous acid concentration reached its maximum value, the fast reaction period (70–170 min) ended, and most of the hydrazine was consumed. During the fast reaction period, part of the hydrazine consumption was a result of the oxidation of Tc(V, VI, and VII) (reactions 1, 2, and 3), and the other part was a result of the reaction of hydrazine with nitrous acid. Although the rate constant k_9 reached 4876 $(mol \cdot min)^{-1}$, which was the fastest chemical reaction in the reaction system, the generation of nitrous acid was controlled by three parallel reactions: reactions 4, 5, and 6. Among them, reaction 4 had the fastest rate, but k_4 was only 1.19 $(mol \cdot min)^{-1}$. Comparatively, the rate constants of reactions 2 and 3 were one order of a magnitude higher than that of reaction 4, and, as Figure 10D–F shows, the concentration of Tc(V) plus Tc(VI) is higher than that of Tc(IV). Therefore, the consumption of hydrazine during the rapid reaction period was mainly attributed to the oxidation of Tc(V, VI). Because of the fast reaction, Tc(IV) + Tc(VII) = Tc(V) + Tc(VI) (reactions 7 and 8), the concentrations of Tc(V) and Tc(VI) in the solution continued to accumulate, further accelerating the consumption of hydrazine. Therefore, an increase in the initial TcO_{4-}^- concentration accelerated the hydrazine oxidation rate.

As the reaction entered the termination period (after 170 min), the nitrous acid concentration reached its maximum and then gradually decreased. This was mainly attributed to the insufficient driving force in the solution to reduce Tc(VII) to Tc(IV) after a considerable amount of hydrazine was consumed, resulting in the inactivation of the Tc(IV, V, VI, VII) catalytic cycle. Figure 10 shows that during the termination period, Tc(IV) can be swiftly oxidized to Tc(V) by nitric acid via reaction 4 (Table 1). Subsequently, Tc(V) and Tc(VI) can rapidly react to yield Tc(VII). Consequently, the net effect of this reaction is a rapid decrease in the concentration of Tc(IV), accompanied by a corresponding increase in the

concentration of Tc(VII). Once the concentration of Tc(IV) approaches zero, the remaining Tc(V) and Tc(VI) present in the solution are gradually oxidized to form Tc(VII) through reactions 5 and 6 with nitric acid. Thus, during the termination period, the concentration of Tc(VII) initially rises quickly before transitioning to a slower rate of increase. The simulation results are consistent with the experimental results, as Figures 2–4 show.

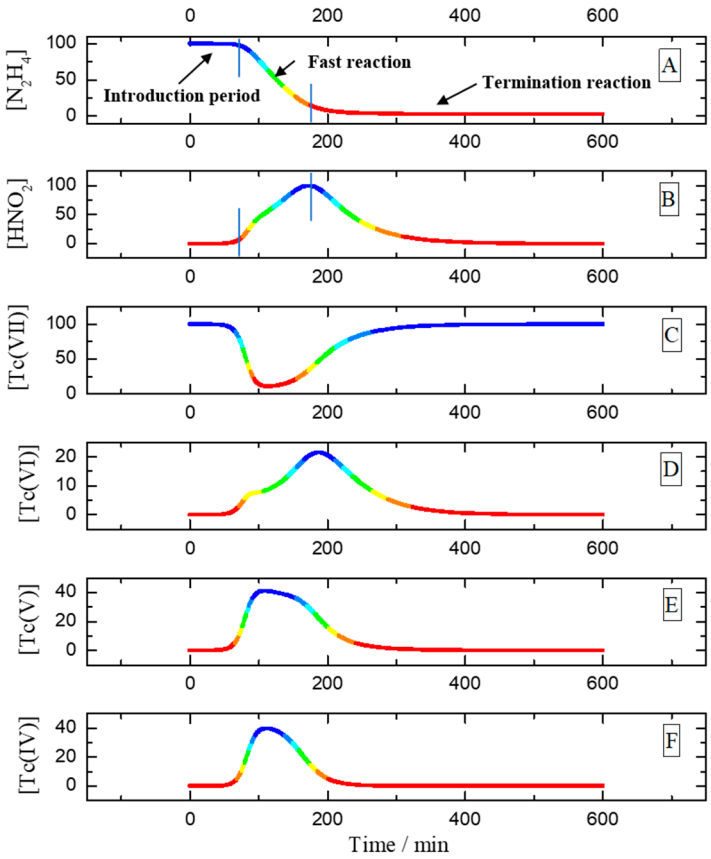


Figure 10. Simulated values of the dependence of Tc and hydrazine concentration on time. $c(TcO_4^-)$ = 1.2 mmol/L, $c(HNO_3)$ = 1.0 mol/L, $c(N_2H_5^+)$ = 0.1 mol/L, T = 35 °C. (**A**–**F**) represent the components hydrazine, HNO_2, Tc(VII), Tc(VI), Tc(V), and Tc(IV), respectively.

5. Conclusions

This study investigated the chemical reaction between hydrazine and Tc. The catalytic reaction of this complex system was investigated by monitoring the concentration changes in hydrazine and Tc(VII) in a nitric acid solution. A kinetic model of the reaction was established, and the fourth-order Runge–Kutta method was used to numerically solve the reaction model and obtain the reaction rate constant. This model accurately predicted the variation in hydrazine concentrations. The results indicated that the reaction between Tc and hydrazine underwent an induction period, a rapid reaction period, and a termination period. During the induction period, Tc(VII) was slowly reduced by hydrazine and Tc(IV, V, VI) gradually accumulated in the solution until it reacted with nitric acid to rapidly generate nitrous acid, marking the beginning of the rapid reaction period. In this phase, Tc(VI) and Tc(V) served as active intermediates, exhibiting an autocatalytic function in the rapid consumption of hydrazine. With the considerable consumption of hydrazine, the reaction entered the oxidation phase, where the Tc(IV, V, VI, VII) catalytic cycle was inactivated, and Tc(IV, V, VI) was slowly oxidized to Tc(VII) by nitric acid. Considering the catalytic behavior of Tc, the research results may be useful for actinide separation processes based on valence control. For example, in the PUREX process, technetium catalyzes the reduction of Np(V) to Np(IV), which is then extracted by TBP to achieve the separation of neptunium.

Supplementary Materials: The following supporting information can be downloaded at: https://www.mdpi.com/article/10.3390/pr12112319/s1, Table S1: Reaction order of each component fitted by the differential method; Table S2: Reaction rate constants for different concentrations of Tc(VII) and hydrazine.

Author Contributions: Conceptualization, H.Z.; Methodology, T.Y.; Software, H.Z.; Validation, T.Y. and H.Z.; Formal analysis, T.Y.; Investigation, T.Y., Y.N., H.L., Z.G., B.W. and Z.C.; Resources, Y.N.; Data curation, T.Y., H.L. and Z.G.; Writing—original draft, T.Y.; Writing—review & editing, H.Z.; Visualization, T.Y.; Supervision, H.Z.; Project administration, Y.N.; Funding acquisition, H.Z. All authors have read and agreed to the published version of the manuscript.

Funding: The paper is sponsored by the National Natural Science Foundation of China (U1867205; 21790371) and the Special Project on Spent Fuel Reprocessing of the State Administration of Science, Technology and Industry for National Defence (BG222512000203).

Data Availability Statement: The original contributions presented in the study are included in the article/supplementary material, further inquiries can be directed to the corresponding author.

Acknowledgments: We greatly appreciate the anonymous reviewers and editors for their constructive comments and valuable advice.

Conflicts of Interest: There are no conflicts of interest to declare.

References

1. Madic, C.; Lecomte, M.; Baron, P.; Boullis, B. Separation of Long-Lived Radionuclides from High Active Nuclear Waste. *Comptes Rendus Phys.* **2002**, *3*, 797–811. [CrossRef]
2. Bonnerot, J.M.; Broudic, V.; Phélip, M.; Jégou, C.; Varaine, F.; Deschanels, X.; Arnoux, M.F.; Faugère, J.L. Transmutation in Reactor and Aqueous Corrosion Resistance of Technetium Metal. *J. Nucl. Radiochem. Sci.* **2005**, *6*, 287–290. [CrossRef] [PubMed]
3. Childs, B.C. *Volatile Technetium Oxides: Implications for Nuclear Waste Vitrification*; University of Nevada, Las Vegas: Las Vegas, NV, USA, 2017.
4. Ashley, K.R.; Whitener, G.D.; Schroeder, N.C.; Ball, J.R.; Radzinski, S.D. Sorption behavior of pertechnetate ion on reillex^{tm}-hpq anion exchange resin from hanford and melton valley tank waste simulants and sodium hydroxide/sodium nitrate solutions. *Solvent Extr. Ion Exch.* **1998**, *16*, 843–859. [CrossRef]
5. Dvoeglazov, K.N.; Marchenko, V.I.; Koltunov, V.S. Oxidation of U(IV) in HNO3 Solutions Containing Urea and Tc(VII). *Radiochemistry* **2005**, *47*, 63–68. [CrossRef]
6. Koltunov, V.S.; Marchenko, V.I.; Nikiforov, A.S.; Smelov, V.S.; Shmidt, V.S.; Gomonova, T.V.; Polunin, A.K.; Kondrat'ev, B.A. The Role Taken by Technetium in the Oxidation-Reduction Processes Used in Irradiated-Fuel Technology. *Sov. At. Energy* **1986**, *60*, 43–51. [CrossRef]
7. Koltunov, V.S.; Gomonova, T.V.; Marchenko, V.I. Kinetics of technetium reactions. V. Reduction of Tc (VII) by uranium (IV) in HCl solution. *Sov. Radiochem.(Engl. Transl.)* **1985**, *26*, 730–734.
8. Garraway, J.; Wilson, P.D. The Technetium-Catalysed Oxidation of Hydrazine by Nitric Acid. *J. Less Common Met.* **1984**, *97*, 191–203. [CrossRef]
9. Melent'ev, A.B.; Mashkin, A.N.; Tugarina, O.V.; Kolupaev, D.N.; Zilberman, B.Y.; Tananaev, I.G. Effect of Some Reducing and Complexing Agents on the Extraction Behavior of Technetium in the TBP-HNO3 System. *Radiochemistry* **2011**, *53*, 256–263. [CrossRef]
10. Melent'ev, A.B.; Mashkin, A.N.; Tugarina, O.V.; Kolupaev, D.N.; German, K.E.; Tananaev, I.G. Effect of Complexing Agents (DTPA and Oxalic Acid) on the Extraction Behavior of Technetium in the TBP-N2H5NO3-HNO3 System. *Radiochemistry* **2011**, *53*, 172–177. [CrossRef]
11. Regalbuto, M.C. 7–Alternative Separation and Extraction: UREX+ Processes for Actinide and Targeted Fission Product Recovery. In *Advanced Separation Techniques for Nuclear Fuel Reprocessing and Radioactive Waste Treatment*; Nash, K.L., Lumetta, G.J., Eds.; Woodhead Publishing Series in Energy; Woodhead Publishing: Oxford, UK, 2011; pp. 176–200.
12. Kumari, I.; Kumar, B.V.R.; Khanna, A. A Review on UREX Processes for Nuclear Spent Fuel Reprocessing. *Nucl. Eng. Des.* **2020**, *358*, 110410. [CrossRef]
13. Marchenko, V.I.; Zhuravleva, G.I.; Dvoeglazov, K.N.; Savilova, O.A. Behaviors of Plutonium and Neptunium in Nitric Acid Solutions Containing Hydrazine and Technetium Ions. *Theor. Found. Chem. Eng.* **2008**, *42*, 733–739. [CrossRef]
14. Ozawa, M.; Ishida, M.; Sano, Y. Strategic Separation of Technetium and Rare Metal Fission Products in Spent Nuclear Fuel: Solvent Extraction Behavior and Partitioning by Catalytic Electrolytic Extraction. *Radiochemistry* **2003**, *45*, 225–232. [CrossRef]
15. Zhou, X.; Ye, G.; Zhang, H.; Li, L.; Luo, F.; Meng, Z. Chemical Behavior of Neptunium in the Presence of Technetium in Nitric Acid Media. *Radiochim. Acta* **2014**, *102*, 111–116. [CrossRef]
16. Sood, D.D.; Patil, S.K. Chemistry of Nuclear Fuel Reprocessing: Current Status. *J. Radioanal. Nucl. Chem.* **1996**, *203*, 547–573. [CrossRef]

17. Marchenko, V.I.; Koltunov, V.S.; Dvoeglazov, K.N. Kinetics and Mechanisms of Redox Reactions of U, Pu, and Np in Tributyl Phosphate Solutions. *Radiochemistry* **2010**, *52*, 111–126. [CrossRef]
18. Mashkin, A.N.; Korchenkin, K.K.; Svetlakova, N.A. Technetium Distribution throughout Purex Process Cycles at RT-1 Plant. *Radiochemistry* **2002**, *44*, 35–41. [CrossRef]
19. Strubinger, S.K.D.; Sun, I.W.; Cleland, W.E., Jr.; Hussey, C.L. Electrochemical and Spectroscopic Studies of Rhenium(IV) Monomeric and Dimeric Chloride Complexes in the Basic Aluminum Chloride-1-Methyl-3-Ethylimidazolium Chloride Room-Temperature Molten Salt. *Inorg. Chem.* **1990**, *29*, 4246–4252. [CrossRef]
20. Hondrogiannis, E.M.; Mamantov, G. Spectroscopy, Electrochemistry, and Spectroelectrochemistry of Rhenium Chlorides in the $AlCl_3$-$NaCl_{sat}$ Melt. *J. Electrochem. Soc.* **1995**, *142*, 2532. [CrossRef]
21. Sekine, T.; Narushima, H.; Suzuki, T.; Takayama, T.; Kudo, H.; Lin, M.; Katsumura, Y. Technetium(IV) Oxide Colloids Produced by Radiolytic Reactions in Aqueous Pertechnetate Solution. *Colloids Surf. A Physicochem. Eng. Asp.* **2004**, *249*, 105–109. [CrossRef]
22. Grey, J.K.; Marguerit, M.; Butler, I.S.; Reber, C. Pressure-Dependent Raman Spectroscopy of Metal-Oxo Multiple Bonds in Rhenium(V) and Osmium(VI) Complexes. *Chem. Phys. Lett.* **2002**, *366*, 361–367. [CrossRef]
23. Rodríguez, D.M.; Mayordomo, N.; Parra-Puerto, A.; Schild, D.; Brendler, V.; Stumpf, T.; Müller, K. Exploring the Reduction Mechanism of 99Tc(VII) in NaClO4: A Spectro-Electrochemical Approach. *Inorg. Chem.* **2022**, *61*, 10159–10166. [CrossRef] [PubMed]
24. Kuznetsov, V.V.; Chotkowski, M.; Poineau, F.; Volkov, M.A.; German, K.; Filatova, E.A. Technetium Electrochemistry at the Turn of the Century. *J. Electroanal. Chem.* **2021**, *893*, 115284. [CrossRef]

Disclaimer/Publisher's Note: The statements, opinions and data contained in all publications are solely those of the individual author(s) and contributor(s) and not of MDPI and/or the editor(s). MDPI and/or the editor(s) disclaim responsibility for any injury to people or property resulting from any ideas, methods, instructions or products referred to in the content.